STRUCTURE OF MEAN WINDS AND TURBULENCE IN THE PLANETARY BOUNDARY LAYER OVER RURAL TERRAIN

H. W. TEUNISSEN

Atmospheric Environment Service, Toronto, Canada

(Received in final form 4 December 1979)

Abstract. A detailed analysis has been carried out of the temporal and spatial structure of mean winds and turbulence in the neutrally-stable planetary boundary layer over typically rural terrain. The data were obtained from a horizontal array of tower-mounted propeller anemometers ($z = 11$ m) during a five-hour period for which the mean wind direction was virtually perpendicular to the main span of the array. Various turbulence characteristics have been obtained for all three components of velocity and have been compared with idealized models for such a flow and with some of the other available atmospheric results.

Considerable tower-to-tower and block-to-block variability has been observed in many of the measured results, particularly in those for the horizontal-component integral scales. Surface shear stress, roughness length and turbulence intensities were in good agreement with expected values for such a site. Power spectra for all components displayed significantly more energy at middle and lower frequencies than that observed by Kaimal *et al.* (1972) over flat, relatively featureless terrain. This is felt to be a result of the generally rougher gross features of the terrain in the present case and has led to the development of a modified version of the Kaimal spectral model which fits the observed data better than either the original Kaimal model or the von Kármán model. It is suggested that it may in future be possible to represent power spectra over a wide range of terrain types by using such a modified spectral model.

Integral scales of turbulence were calculated by three different techniques and in most cases displayed a strong dependence on the technique used. Averaged values of scale showed reasonable agreement with most of the available atmospheric data and with the values suggested by ESDU (1975). The anticipated elongation of turbulent eddies in the longitudinal direction was confirmed for all three velocity components, although it was found to be not as large as some other observations.

Nomenclature

a_i, b_i	spectral equation constants – see Section 3.5
f	non-dimensional frequency $= nz/\bar{U}$
k	wave number $= n/\bar{U}$
k_p^i	wave number at which peak of i-component power spectrum occurs
K_{10}	surface drag coefficient ($z = 10$ m) $\equiv (u_*/\bar{U}_{10})^2$
l_i^j	integral scale of i-component for separation in j-direction, calculated by correlation integral technique (Section 3.7)
$\hat{l}_i^j$	integral scale of i-component for separation in j-direction, calculated by exponential fit technique (Section 3.7)
L_i^j	integral scale of i-component for separation in j-direction, calculated by spectral fit technique (Section 3.7)
n	frequency
n_c	filter cut-off frequency (−3 dB)
Ri_g	gradient Richardson number
$\tilde{R}_i\ (\Delta y, \tau)$	normalized time-delayed cross-correlation of i-components for separations in lateral direction [e.g. $\tilde{R}_u\ (\Delta y, \tau) = \overline{u_1 u_2}/(\sigma_{u_1}\sigma_{u_2})$]
$\tilde{R}_i\ (\tau)$	normalized autocorrelation of i-component [e.g. $\tilde{R}_u(\tau) = \overline{u(t)\ u(t+\tau)}/\sigma_u^2$]
$\tilde{R}_{ij}(0)$	Reynolds stress coefficient for i- and j-components [e.g. $\tilde{R}_{uw}(0) = \overline{uw}/(\sigma_u\sigma_w)$]
$S_i\ (n)$	power spectral density of i-component
t	time

Boundary-Layer Meteorology **19** (1980) 187–221. 0006-8314/80/0192-0187$05.25.

Δt	sampling period
T_B	data block length
T_i	turbulence intensity of i-component $= \sigma_i / \bar{U}$
u, v, w	longitudinal, lateral and vertical turbulence velocity components, respectively
u_m, v_m, w_m	velocity components in anemometer reference frame
u_*	friction velocity $= \sqrt{-\overline{uw}}$
$\bar{U}$	magnitude of mean wind velocity vector
x, y, z	longitudinal, lateral and vertical coordinate directions, respectively
z_0	surface roughness length
Δy	lateral separation
$\bar{\phi}$	azimuthal direction of mean wind velocity vector
σ_i	standard deviation of i-component
τ	time-delay for correlations
Subscript $(_i)$	refers to velocity component u, v or w
Subscript $(_{AVG})$	refers to average over all towers in a data block
Superscript $(^l)$	refers to direction x, y, z

1. Introduction

In past years, many measurements have been made of the wind and turbulence structure in the atmospheric or planetary boundary layer (PBL). Such measurements are of course essential for developing a suitable description and understanding of the basic nature of these flows for application to a wide variety of problems. In the field of wind engineering, for example, problems such as wind loading on buildings, bridges and other structures, wind effects on slow and low-flying aircraft, transmission line oscillation and the dispersal of atmospheric pollutants are intimately dependent on the characteristics of the PBL over various types of surface terrain.

Many known characteristics of the PBL have been obtained from meteorological research programs aimed at studying the basic physics of the flows. Measurements of turbulence structure and exchange coefficients over relatively large, flat, idealized surface areas during various conditions of atmospheric stability (e.g., Clarke, 1970; Kaimal *et al.*, 1972; Kaimal *et al.*, 1976; etc.) have led to similarity theories which describe the flow over these surface types quite well. Considerably less information is available concerning the spatial structure of the turbulence in the planetary layer, however, particularly over rougher, less ideal terrain types and for separations in the horizontal direction. Some results are of course available (e.g., Panofsky, 1962; Elderkin *et al.*, 1972; Harris, 1972; Ropelewski *et al.*, 1973; Shiotani and Iwatani, 1976; Shiotani *et al.*, 1978; Perry *et al.*, 1978; Flay, 1978) and many of these have been included in the numerous comprehensive reviews of existing data which have been produced in both the engineering and meteorological literature (e.g., Lumley and Panofsky, 1964; Teunissen, 1970; Busch *et al.*, 1973; ESDU, 1974 and 1975; Counihan, 1975; Panofsky, 1977). A common feature of virtually all of these reviews, however, is that they have demonstrated a clear need for additional full-scale measurements of the spatial structure of turbulence in the PBL over all types of terrain.

In response to the above requirements, an existing array of towers in a typically rural area has been instrumented to allow the measurement of wind and temperature

at various points around the site, and thereby to permit detailed studies of the spatial structure of the PBL over terrain of this type. Separate horizontal and vertical arrays of anemometers are located at the site, along with a computer-orientated data acquisition and analysis system. In the present paper, a brief description of the measurement and analysis facility is presented, followed by a detailed analysis of the temporal and spatial structure of the winds and turbulence measured by the horizontal anemometer array during a five-hour period when the mean wind vector was nearly perpendicular to the array and was sufficiently large to produce a flow with virtually neutral thermal stability. Such neutrally-stable flows are of most interest in the wind-loading-type of problem referred to earlier, since these problems usually become serious only at the relatively high wind speeds during which the atmosphere may in fact reasonably be assumed to be neutrally stable. In addition to mean wind

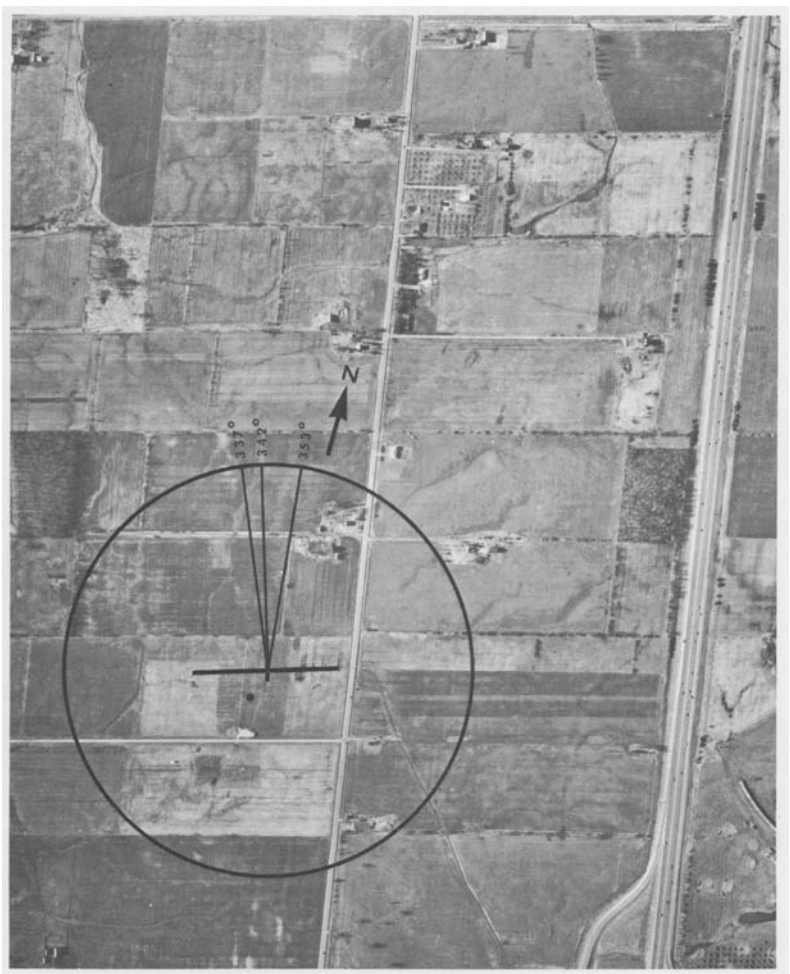

Fig. 1. Aerial view of site.

speeds and directions, turbulence intensities, Reynolds stresses, autocorrelations, power spectra, cross-correlations and integral scales are presented for all three components of turbulence velocity and for various towers and combinations of towers. Such results are compared with both the predictions of idealized engineering models of the PBL and with some of the available atmospheric measurements for similar flows. Coherence results will also be obtained for this data set and will be presented in a subsequent publication. Results for other wind directions and stability conditions will also be presented at a later time.

2. Measurement Facility and Data Handling Procedures

A brief description of the measurement facility and data handling procedures is presented in this section. Full details, including program listings, have been described by the author in a separate report (Teunissen, 1977).

2.1. Tower array and site details

The tower array is situated on what was originally a farm site located about 20 km northwest of the city of Toronto, Canada, near the town of Woodbridge. The terrain is relatively flat and open and the surface is characterized by grass and occasional trees or groups of trees and farm buildings (Figure 1). Typical surface roughness lengths of the order of several centimeteres would be expected in the summer time, with lower values in winter when the ground is usually covered with snow. Fifteen 11-m towers and one 50-m tower are located on the site as shown schematically in Figure 2. Two semi-permanent trailers are also located on the site and house the analog and digital equipment needed for complete collection, storage and analysis of the measured data.

2.2. Instrumentation

The 11-m towers form a basic straight-line array and have Gill UVW Propeller Anemometers (Model 27004) mounted atop them as can be seen in Figure 3. In addition, most towers have Canadian standard U2A cup-and-vane anemometers mounted on them, although these were not used for any of the results to be discussed in this paper. The Gill anemometers were aligned with a simple level and sighting device in such a way that the w-arm is vertical, the v-arm is parallel to the main, 300-m length of the 11-m tower array and the u-arm is perpendicular to this length. The accuracy of these alignment procedures is estimated to be about $\pm 0.5°$. Four-bladed, 23-cm-diameter, polystyrene propeller blades are used for all velocity components.

The response characteristics of the Gill UVW anemometer have been discussed extensively in the literature and are now well-understood (e.g., Hicks, 1972; Horst, 1973; etc.). In the present case, non-cosine-response corrections were applied to all the data using the technique described by Horst (1973). The upper frequency response limit (-3dB) for these measurements is estimated to be about 0.8 Hz for the

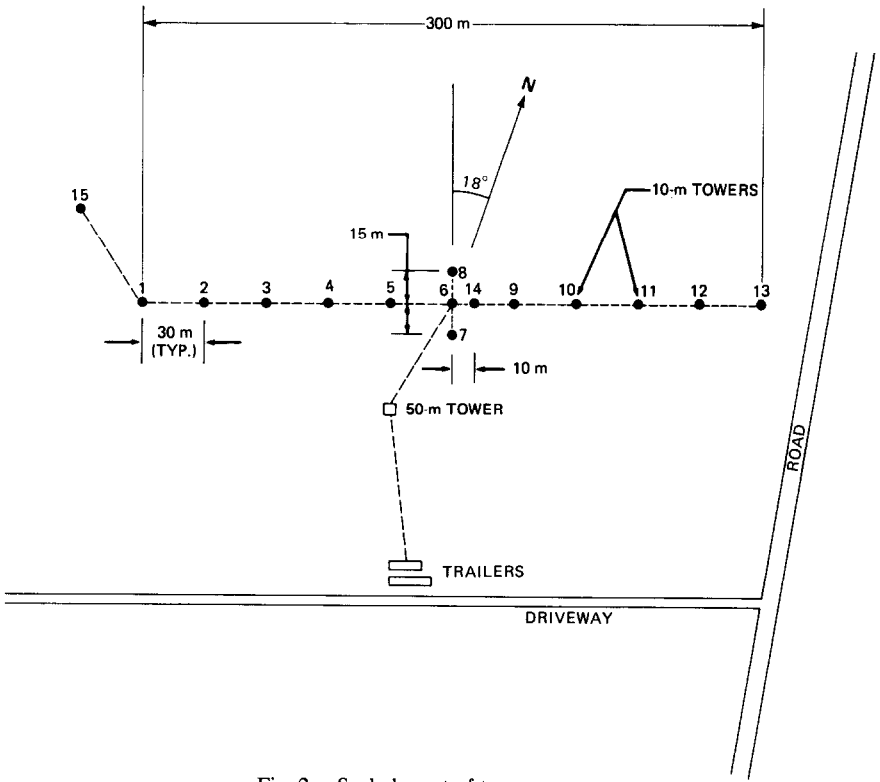

Fig. 2. Scale layout of tower array.

Fig. 3. View along 10-m tower array (looking ENE).

horizontal components and 0.3 Hz for the vertical component (see also Section 3.3 and Teunissen, 1977).

The 50-m tower (Figure 4) is presently instrumented at 7 levels (5, 7, 10, 20, 30, 40 and 50 m above the surface) with Bendix Aerovanes and platinum resistance temperature sensors mounted on horizontal booms which extend about three tower widths away from the tower itself. The Aerovanes were not used for the present

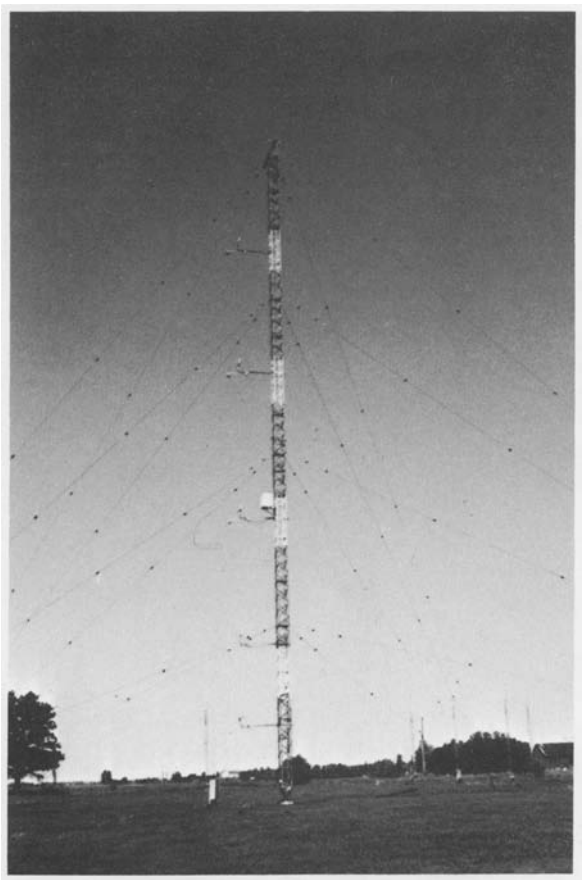

Fig. 4. View of 50-m tower (looking north).

experiment. The temperature sensors are Rosemount Model 78–0039–007 platinum resistance elements mounted in Teledyne–Geotech Model 327 aspirated radiation shields. The sensors are connected to Rosemount Model 414L3AGA linear bridges which are located in one of the instrumentation trailers. It is estimated that absolute temperature measurements are accurate to ±0.15 °C using this system, while temperature differences are accurate to ±0.05 °C. The time constant of the system is of the order of 5 s, so that only mean temperatures are attainable.

2.3. Data collection and analysis

Data collection and analysis are performed at the site as two distinct operations separated by interim storage of digital data on 9-track magnetic tape, as depicted in Figure 5. Both the collection and analysis systems are built around a PDP–15 digital computer and its associated peripheral equipment located in one of the trailers. In the collection phase, analog signals from the various sensors are sent to the trailers

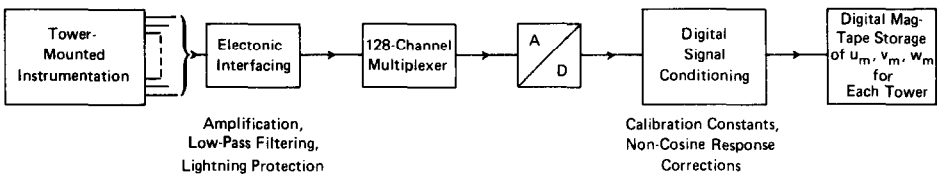

(A) DATA COLLECTION AND STORAGE

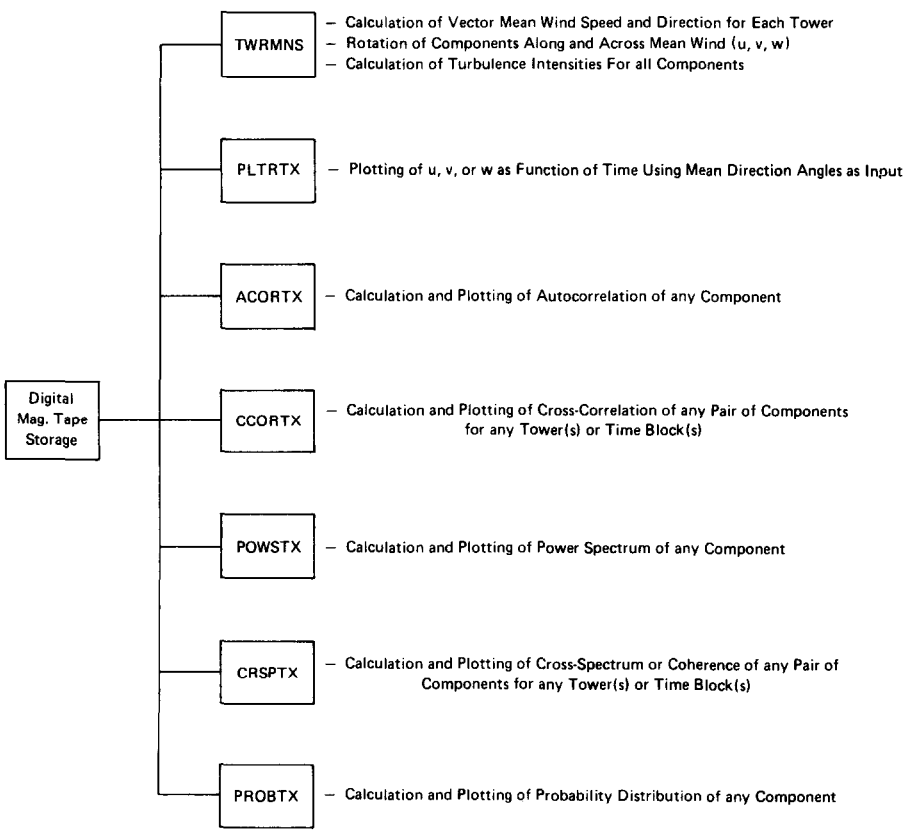

(B) DATA ANALYSIS PROGRAMS

Fig. 5. Block diagram of data collection and analysis systems.

via buried, shielded cables. An analog interface amplifies and filters these signals prior to their entering the 128-channel multiplexer and subsequently the A/D converter. A double-buffer approach is used for collecting the digitized data so that calibration constants and non-cosine-response corrections can be applied to one full buffer while a second is being filled with new data. Such a system permits continuous storage of corrected, digitized velocity components from all towers and hence saves time in subsequent analysis.

The data analysis system consists of a set of Fortran programs which reads the velocity data from the digital tapes, performs the statistical calculations outlined in Figure 5 and outputs the resulting information on an alphagraphic printer. It can be used for data collected from other sites (e.g., Teunissen, 1979) provided the storage format for the data is appropriately chosen. Block lengths of up to 4096 samples per velocity component may be chosen in integral powers of 2. Standard statistical procedures are used to calculate the quantities outlined in Figure 5, and details of these are given by Teunissen (1977).

The velocity components stored on digital tape are necessarily those in the anemometer reference frame (u_m, v_m, w_m), since prior to analysis the mean wind direction is of course not known. The first stage in statistical analysis is therefore to calculate the direction of the mean wind vector for each block and anemometer. These directions are then used in all subsequent analyses to rotate the measured components into a reference frame with the x-axis along the mean wind direction and the y-axis in the horizontal plane. The resulting longitudinal (u), lateral (v) and vertical (w) velocity components are then such that $\bar{u} = \bar{U}$ and $\bar{v} = \bar{w} = 0$, as conventionally defined (see also Section 3.2).

3. Results and Discussion

3.1. Data

The wind data to be discussed in this paper were obtained from 11 of the 15 10-m towers in the horizontal array (numbers 1, 2, 3, 4, 5, 6, 7, 9, 10, 11 and 14 in Figure 2) during a 5-h period beginning at 1400 LST (1900Z) on the afternoon of March 22, 1977. A region of low pressure had developed over the state of North Carolina at about 0700 h and had moved from eastern Maryland at about 1300 h to Long Island, N.Y., by 1900 h. This low produced strong, northerly winds, overcast skies (ceiling about 500 m) and light snow in the Toronto area throughout the measurement period. The ground was snow-covered and a considerable amount of blowing snow was encountered. The ambient temperature remained relatively constant throughout the period, dropping only from −1 °C at 1300 h to −2 °C at 1900 h. Sunset occurred at 1830 h. From this information and nearby radiosonde data, the boundary layer was expected to be neutrally stable up to an inversion height of 400–500 m.

Two mean temperature profiles were obtained from the 50-m tower between 1400 and 1500 h. Using the temperature gradient from these profiles, the average value of

u_* from uw cross-correlation measurements (Section 3.3) and assuming the applicability of the log-law for determining the mean velocity gradient at $z = 11$ m, a typical gradient Richardson number of $\mathrm{Ri}_g \sim +0.005$ was obtained, thereby confirming the near-neutral stability of the lower regions of the boundary layer.

A sampling rate of 1.71 s^{-1} ($\Delta t = 0.5833$ s) was used for the present measurements in view of the known response characteristics of the Gill anemometers and the analog filters. A nominal data block length of 2048 samples was chosen, corresponding to $T_B = 1195$ s or 19.9 min. Such a block length is usually considered sufficiently long to extend into the so-called 'spectral gap' region of the horizontal velocity power spectrum. Some of the data presented here were also investigated using a block length of 4096 samples, and no significant changes in the results were observed.

3.2. Mean wind speed and direction

The variation of the magnitude and direction of the mean wind vector for each data block, averaged over all towers in the array, is shown in Figure 6. The 19.9-min data blocks have been identified consecutively by the numbers 1 through 12. In all subsequent figures of this paper, numbered curves or data points refer to these block numbers. The gap between 1500 and 1600 h occurred only because the system was shut down during this period.

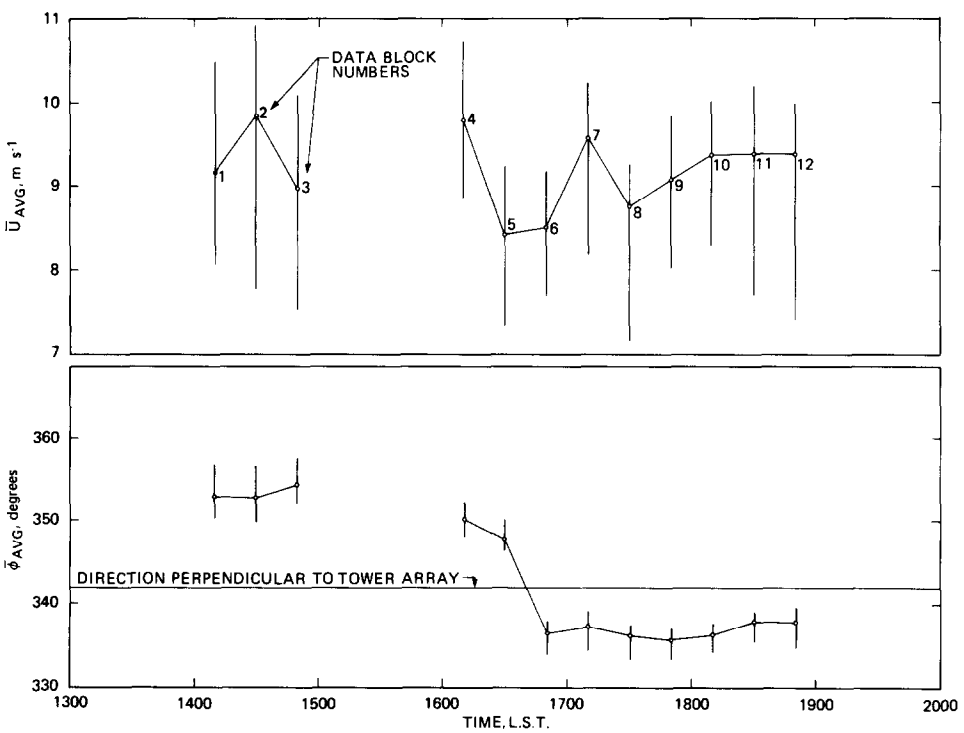

Fig. 6. Variation of block-mean wind speed and direction with time (data averaged over all towers).

The average wind speed for all twelve blocks was 9.19 m s^{-1}. It can be seen in Figure 6 that the individual block-mean speeds remained within about 8% of this value throughout the afternoon, thereby suggesting reasonable stationarity of the data for the entire measurement period. On the other hand, the direction results show a distinct backing of the wind from about 353° before 1600 h to about 337° after 1700 h. These results clearly indicate that the data should be treated as two separate, individually-stationary sets of data, one for $\bar{\phi}_{AVG} \sim 353°$ (blocks 1–3) and one for $\bar{\phi}_{AVG} \sim 337°$ (blocks 7–12, say). It will therefore be interesting to compare certain features of each group of blocks in order to try to identify possible effects of the slightly different upstream fetches for the two cases.

The vertical bars shown in Figure 6 for each block-mean value represent the total range of these values for each of the 11 towers in the array. Part of the observed variability can be attributed to anemometer calibration differences, while part is presumably due to real spatial variation in the wind characteristics. In Figure 7, the

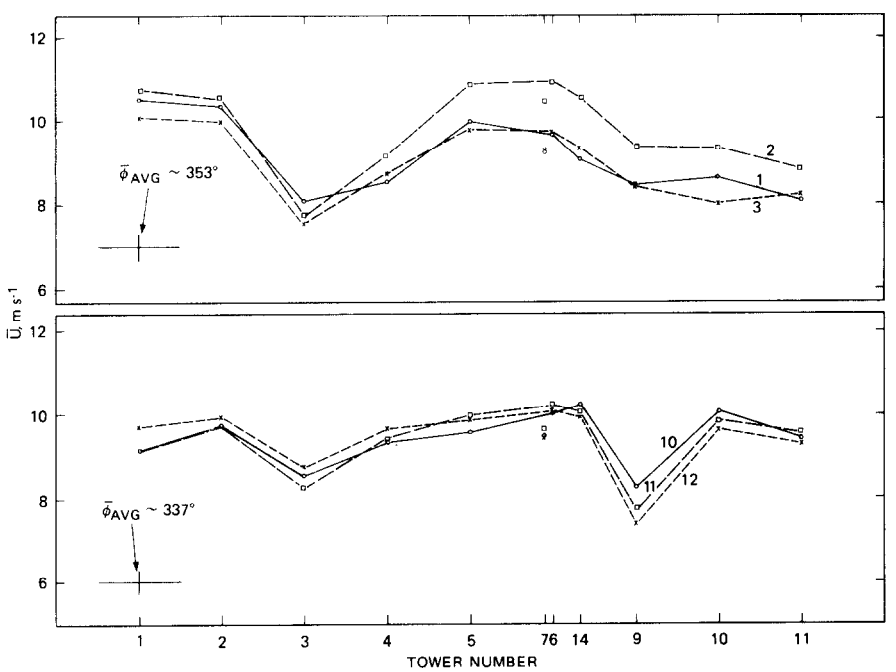

Fig. 7. Variation of mean wind speed over tower array for several typical data blocks.

individual block-means for all towers are plotted for each of six typical data blocks. A distinct spatial pattern is evident for data blocks 1 to 3 ($\bar{\phi}_{AVG} \sim 353°$) and it is clear that this pattern changes for the different mean direction represented by blocks 10–12 ($\bar{\phi}_{AVG} \sim 337°$). It was originally estimated that the instrumentation errors involved in determining $\bar{U}$ should be less than about ±5%, an estimate which is substantiated by the roughly 6% total difference between the values for towers 6 and

7 in Figure 7. These towers are located virtually one behind the other for these wind directions and should therefore presumably indicate identical values. (Note that tower 7 results in Figure 7 and similar figures are plotted at a slightly displaced abscissa value relative to tower 6 so as to minimize confusion in displaying the results). It is nevertheless questionable whether the roughly 20% drop displayed by towers 3 and 9 are real spatial effects or merely instrument errors, even though the different patterns for the two sets of data blocks suggest that they are real. In order to investigate this possibility, anemometer calibration corrections were obtained from a completely independent data set (January 17, 1977) for which the mean wind direction was within 10° of being parallel to the tower array and for which all mean speeds should therefore be identical (except, perhaps, for tower 7). Correction factors for each tower were obtained by dividing its mean speed by the array average for each of several data blocks. The average correction factors were within the estimated limit of ±5% for all towers except numbers 3 (−16%) and 11 (+10%). The effects of calibration errors on the spatial patterns of Figure 7 were then removed by scaling these results by the appropriate correction factors, and the resulting data have been plotted in Figure 8.

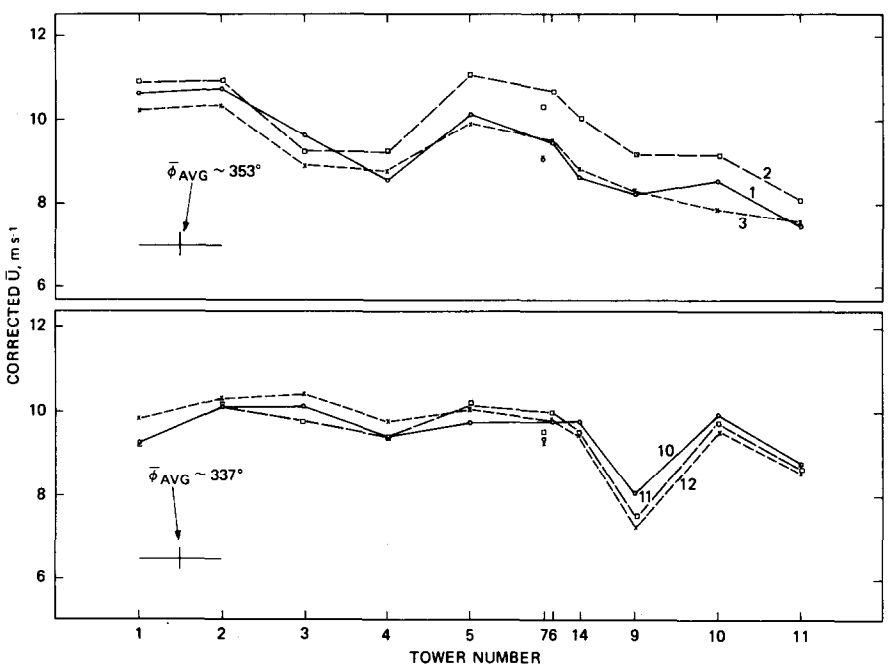

Fig. 8. Data as in Figure 7, but with speeds corrected to remove calibration error effects.

It is clear from Figure 8 that the basic spatial wind patterns observed in Figure 7 were in fact real and must therefore be the result of detailed features of the upstream terrain. The low speeds observed for towers 3 and 4 in blocks 1–3 may have been caused in part by a single, leafless tree located about 60 m upstream of these towers

for this wind direction, and in part by wake effects from a group of farm buildings and trees about 300 m upstream of towers 10–13 for this direction (see Figure 1). The low speeds displayed by towers 9 to 11 for these blocks are no doubt caused by the wake of the farm buildings. For data blocks 10–12, the spatial distribution of wind speed is virtually uniform, except for tower 9. The fact that towers 4 and 5 do not show a significant decrease in speed for this wind direction suggests that the decrease in towers 3 and 4 for blocks 1–3 was in fact an effect of the farm buildings and not of the upstream tree. The slightly low value for tower 11 is probably also a building wake effect, although this effect is quite small. The most significant effect here is obviously the large (~20%) drop in mean speed displayed by tower 9. The possibility that the anemometer calibration may have changed toward the end of the measurement period was rejected, since a subsequent data set (April 5, 1977) with the wind nearly parallel to the tower array, did not show similarly low values for this tower. Since no other potential upstream causes could be identified, it is concluded that this effect must have been caused by the wake of the farm buildings, perhaps corresponding to the low value for tower 4 with $\bar{\phi}_{AVG} \sim 353°$. As for the variation of mean wind direction over the tower array, the results of Figure 9 show that this was quite small, particulary for data blocks 10–12.

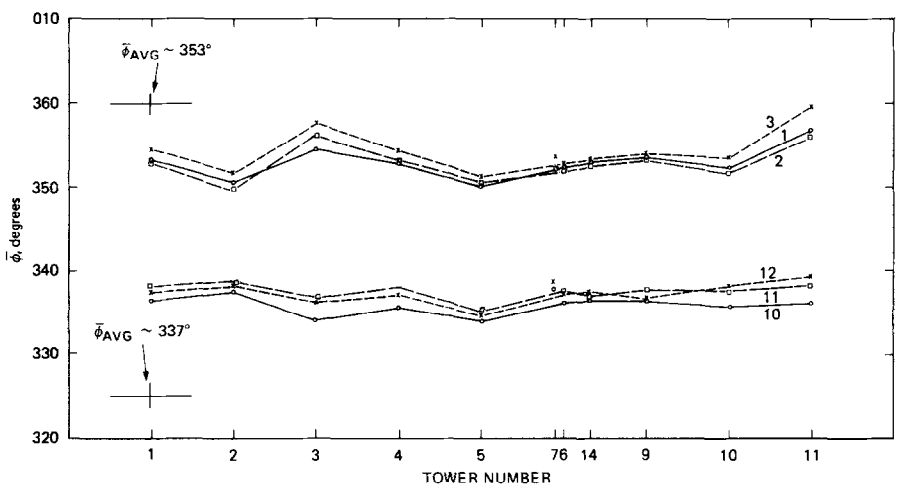

Fig. 9. Variation of mean wind direction over tower array for data blocks 1–3 and 10–12.

In spite of the above spatial effects, data from all 11 towers have been included in all tower-averaged results for each data block presented in this paper. This consititutes an effective assumption of horizontal homogeneity and is felt to be not unreasonable. This is particularly so in the case of data blocks 7–12, as evidenced by the results discussed above and in the following section for blocks 10–12.

Calculations of the block-mean values of wind elevation angle relative to the plane of the anemometer u–v arms yielded angles which for the most part were within the

estimated accuracy of vertical alignment of the anemometers (±0.5°), although a few larger values were observed. In general, these angles were found to have an insignificant effect on the turbulence characteristics obtained for each tower, and the raw turbulence components were not rotated to remove them. The one major exception to this generality was the estimated value of the $\overline{uw}$ cross-correlation for each anemometer. Such cross-correlations are known to be affected by as much as 10–12% per degree of vertical misalignment (e.g., Kaimal and Haugen, 1969; Dyer *et al.*, 1970), an error estimate which was confirmed by comparisons of rotated and non-rotated data in the present case. Thus rotation by the mean elevation angle to ensure that $\bar{w}$ became identically zero was carried out for all $\overline{uw}$ results presented here.

3.3. Turbulence intensities and Reynolds stresses

Figure 10 shows the variation of the tower-averaged turbulence intensities for each data block as a function of time through the measurement period, along with the scatter bars representing the tower-to-tower variability within each block. As expected, the largest temporal variability occurred between 1600 and 1700 h (blocks 4–6) when the mean wind direction was changing. As also expected, the vertical component intensity, T_w, displays significantly less variability than that for the horizontal components as a result of the relative absence of the larger-scale, low-frequency fluctuations which are normally found in the other components.

Figure 10 also displays the turbulence intensity values obtained for the logitudinal velocity component after 'detrending' of the data. Detrending, in the form of subtracting from the raw velocity data for a particular block the best-fit linear (or

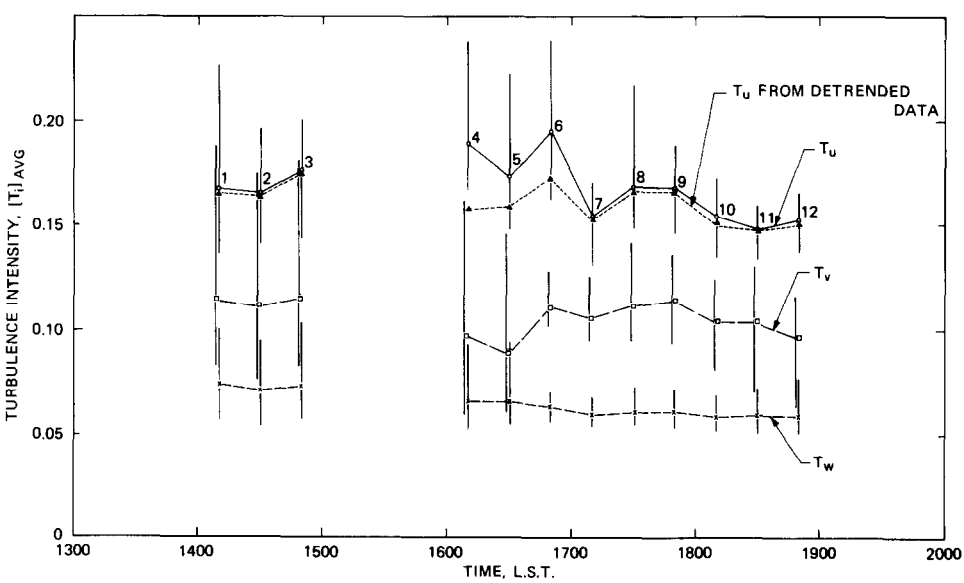

possibly higher-order) regression line for these data, is usually done in an attempt to remove unwanted trends or long-term drifts from the measured atmospheric data. In the present case, trends were not a significant feature, except perhaps for data blocks 4–6. Thus in Figure 10, for example, no significant differences are oberved between detrended and non-detrended turbulence intensities for the u-component for any blocks other than 4, 5 and 6, and these differences are clearly a result of the change in the mean wind direction observed in Figure 6. The corresponding v- and w-component intensities for the detrended data are not shown in Figure 10 because they are virtually coincident with the non-detrended results for all blocks. Similarly, no significant effects of detrending were observed for any other turbulence characteristics in any data blocks other than 4, 5 and 6, and only minor effects were observed in these blocks. Detrending was therefore not used for any of the results presented in this paper unless specifically mentioned.

Tower-averaged Reynolds stress coefficients are shown in Figure 11 for all components and data blocks. These coefficients were obtained by dividing zero-time-delay cross-correlations of the appropriate velocity components by their corresponding standard deviations. In idealized models of planetary surface layer flow over a relatively uniform surface of this type, values of $\tilde{R}_{uv}(0)$ and $\tilde{R}_{vw}(0)$ are assumed to be small or zero and estimates for $\tilde{R}_{uw}(0)$ range from -0.27 (ESDU, 1974) to -0.31 (Teunissen, 1970) or -0.32 (Counihan, 1975). The measured coefficients are seen in Figure 11 to be quite close to these values, except perhaps for the relatively large values of $\tilde{R}_{uv}(0)$ for data blocks 8–11. No explanation for these

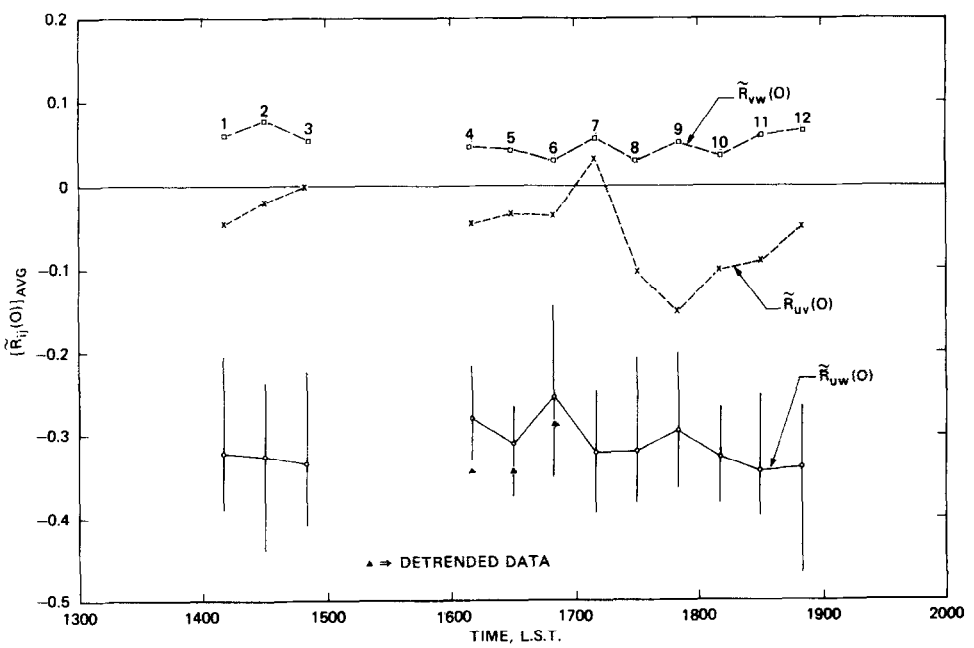

Fig. 11. Variation of Reynolds stress coefficients with time (data averaged over all towers).

larger values could be found. The three values shown for detrended data in the figure are the only ones which differed significantly from the non-detrended values.

Figure 12 shows the spatial characteristics of the measured values of turbulence intensity for all three velocity components for data blocks 1–3 and 10–12. As was the case for mean velocities (Figure 8), there is clearly more spatial variability in the turbulence intensities for blocks 1–3 ($\bar{\phi}_{AVG} \sim 353°$) than for blocks 10–12 ($\bar{\phi}_{AVG} \sim 337°$). This can again be attributed to the upstream farm buildings, which have a more significant impact for the former direction than for the latter. A plot of the standard deviations for all the data shown in Figure 12 (i.e., without the velocity

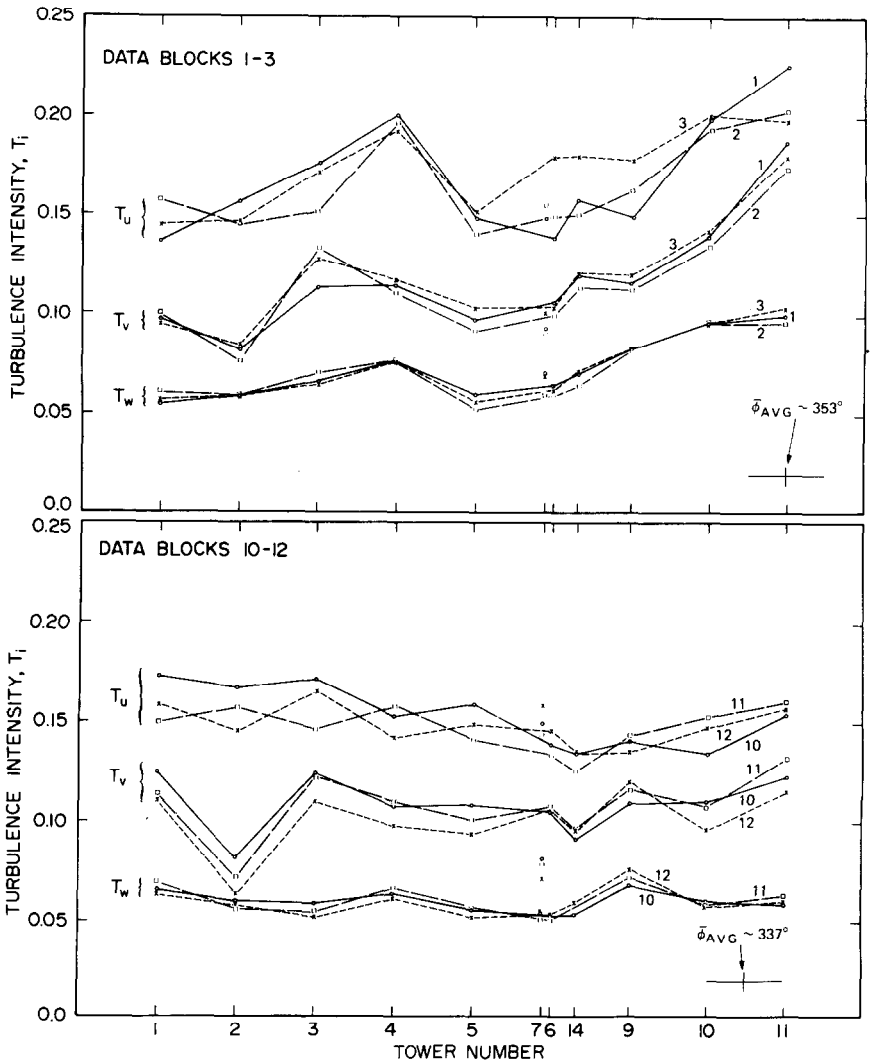

Fig. 12. Variation of turbulence intensities over tower array for data blocks 1–3 and 10–12.

normalization included) displayed spatial patterns substantially the same as those of Figure 12.

In view of the relative uniformity of the upstream fetch for $\bar{\phi}_{AVG} \sim 337°$ (Figure 1) and the relative freedom of the velocity and turbulence results from specific upstream details for this direction, only the data from blocks 7 through 12 will be presented for subsequent discussion of correlations, spectra and integral scales. Block-by-block analysis has been carried out, as well as averaging of block-mean values over all 6 blocks. Data from the other blocks were also studied, and no unexpected results were observed.

If the surface shear stress is assumed for the present data set to be constant from the surface up to at least $z = 11$ m, then the zero-time-delay $\overline{uw}$ cross-correlations can be used to obtain an estimate of the friction velocity u_* for each data block. Also, assuming the validity of the log-law for the mean velocity profile, estimates of the surface drag coefficient, K_{10}, and the roughness length, z_0, can be obtained. These values are tabulated in Table I along with the mean speeds, the $\overline{uw}$ Reynolds stress

TABLE I
Surface and turbulence parameters for data blocks 7–12

Block Number	$\bar{U}$, m s^{-1}	$\tilde{R}_{uw}(0)$	u_*, m s^{-1}	$K_{10}\times10^3$	z_0, cm	σ_u/u_*	σ_v/u_*	σ_w/u_*
7	9.58	−0.323*	0.523	3.1	0.72	2.82	1.94	1.10*
8	8.76	−0.320*	0.507	3.5	1.10	2.92	1.94	1.07*
9	9.08	−0.295*	0.499	3.1	0.77	3.06	2.09	1.11*
10	9.38	−0.327*	0.511	3.1	0.71	2.83	1.93	1.08*
11	9.38	−0.345	0.519	3.2	0.80	2.67	1.88	1.08*
12	9.38	−0.340*	0.520	3.2	0.81	2.76	1.75	1.06*
AVERAGE	9.26	−0.325* (−0.28)	0.513	3.2	0.82	2.84	1.92	1.08* (1.27)
Teunissen (1970)		−0.31	–	–	–	2.5	2.0	1.3
ESDU (1974)		−0.27	–	3.0	≈1	2.97	1.94	1.27
Counihan (1975)		−0.32	–	3.6	0.1–2	2.50	1.88	1.25

* unadjusted for vertical component frequency response limitations.
More probable estimates are bracketed.

coefficients and the ratios σ_i/u_* for each of the six data blocks and for their averages. Also shown for comparison are the idealized model values suggested in several of the reviews referred to earlier for terrain of this type. It is seen that the block-to-block variability of these quantities is relatively small and that the average values for the six blocks compare favourably with most model values, and in particular with those of ESDU (1974). The relatively low values for σ_w/u_* are attributed to the poorer frequency response of the vertical anemometer in comparison with that of the horizontal ones (Section 2.2) as a result of its permanent orientation perpendicular to the mean wind direction. In addition, the higher frequencies normally found in the

vertical component mean that frequency response limitations have a relatively larger impact on it than on the other components. For the anemometer height and mean wind speed observed here, the results of Hicks (1972) and Horst (1973) suggest that u_* and σ_u are underestimated by less than 2% as a result of frequency response limitations, σ_v may be underestimated by up to 10% and σ_w by up to 25%. From the results of Table I, it would appear that σ_v may not be significantly under-estimated, while an upward adjustment of about 18% would bring σ_w into the range of the model values. Such a correction to σ_w would also reduce the average value for $\tilde{R}_{uw}(0)$ to about -0.28, which is again closest to that suggested by ESDU (1974). It therefore appears that an adjustment of this order is reasonable when absolute levels of σ_w or σ_w/u_* are of interest (see Section 3.5).

Finally, it is noted that the block-averaged turbulence intensities for the six blocks of Table I are $\sigma_u/\bar{U} = 0.158$, $\sigma_v/\bar{U} = 0.106$ and $\sigma_w/\bar{U} = 0.060$ (raw result) or 0.071 (corrected).

3.4. Autocorrelations

Autocorrelation curves averaged over all towers in the array are shown in Figure 13 for each of data blocks 7 through 12. The block-to-block variability of these curves is seen to be not too large, particularly for the w-component. It is largest for the u-component, where it is seen that the tail of the curve is not particularly well-behaved in its approach toward zero even though no trends were observed in these data. Such variability can of course be reduced by averaging the curves for all six blocks, and this has been done in obtaining some of the integral scale values discussed in Section 3.7. The general shape of the autocorrelation curves displays the anticipated exponential-type decay with delay time, with the more rapid decay for the v- and w-components being indicative of their relatively smaller integral scales.

Figure 14 shows the range of variability of the autocorrelation curves for all the towers in data block 12. One would expect this variability to be larger than that displayed in Figure 13 for the tower-averaged data, since averaging of individual curves is carried out prior to determining the ranges shown in the latter figure but not in the former. A comparison of the two figures shows that tower-averaging has in fact significantly reduced the variability only in the case of the vertical autocorrelation curves.

3.5. Power spectra

The range within which the tower-averaged power spectra for blocks 7–12 were observed is shown in Figure 15 for all three velocity components. In all cases, the variability in the spectra is seen to decrease with increasing frequency. This is a natural consequence of the averaging approach for raw spectral estimates which was used for all power spectra in order to produce final estimates which are equi-spaced on a logarithmic frequency axis. For the basic block size of 2048 samples used in the present case, the highest-frequency spectral estimate is an average of about 380 raw values and the lowest-frequency estimate is a single raw value. The corresponding

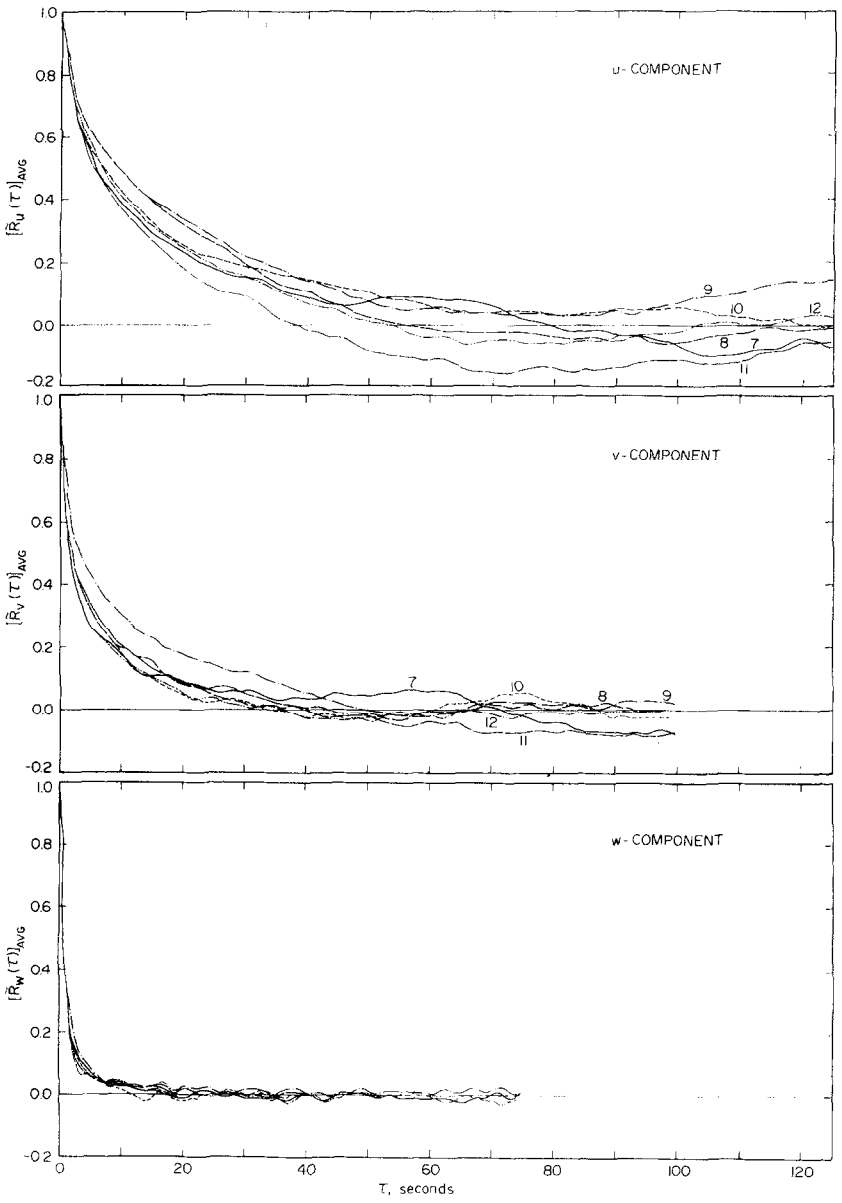

Fig. 13. Tower-averaged autocorrelation curves for data blocks 7–12.

statistical variabilities of these estimates for the power spectra from a single anemometer are about 5% and 100%, respectively (Teunissen, 1977).

A number of empirical or semi-empirical relations have been suggested in the past for representing power spectra in the neutrally-stable PBL. Two commonly used sets of these relations are the von Kármán expressions recommended by Teunissen

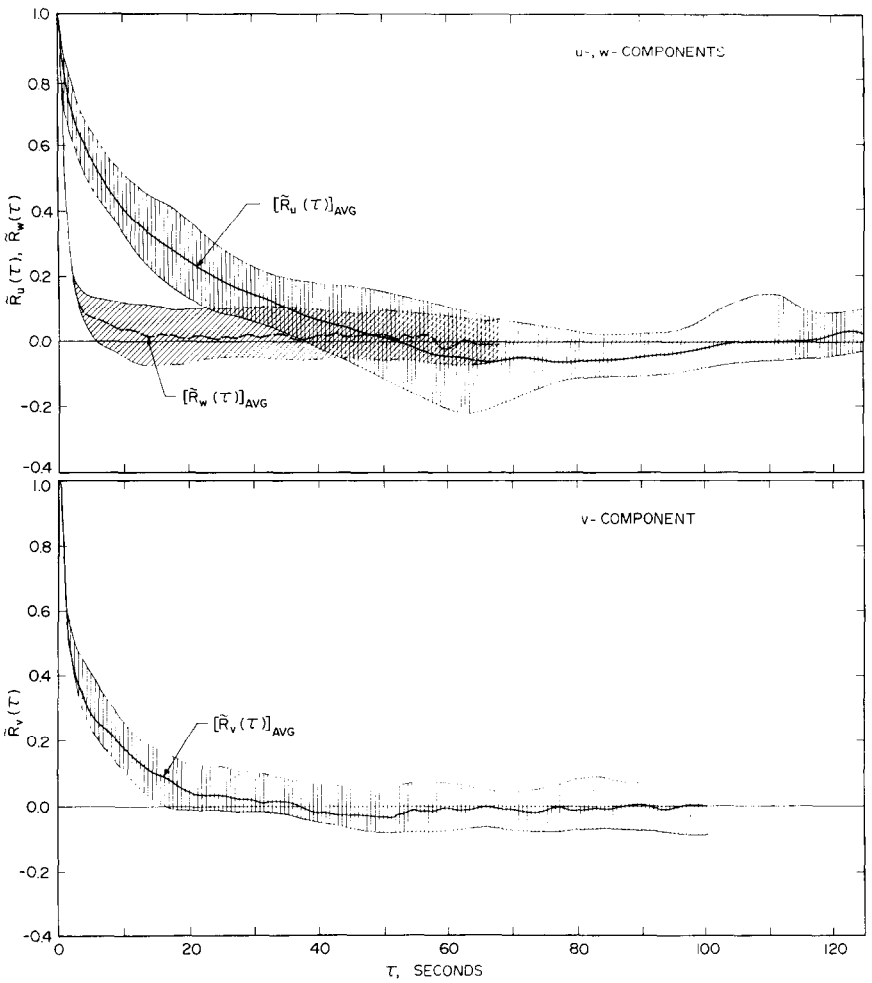

Fig. 14. Range of variation of observed autocorrelation curves over tower array for data block 12.

(1970) and ESDU (1974) for the entire PBL and those of Kaimal *et al.* (1972) for the surface layer over flat, uniform terrain. The von Kármán expressions were originally postulated for isotropic turbulence ($L_u^x = 2L_v^x = 2L_w^x$) and are given by

$$\frac{nS_u(n)}{\sigma_u^2} = \frac{4kL_u^x}{[1+70.7\,(kL_u^x)^2]^{5/6}} \tag{1(a)}$$

$$\frac{nS_v(n)}{\sigma_v^2} = 4kL_v^x\left\{\frac{1+188.4(2L_v^x k)^2}{[1+70.7(2L_v^x k)^2]^{11/6}}\right\} \tag{1(b)}$$

and

$$\frac{nS_w(n)}{\sigma_w^2} = 4kL_w^x\left\{\frac{1+188.4(2L_w^x k)^2}{[1+70.7(2L_w^x k)^2]^{11/6}}\right\}. \tag{1(c)}$$

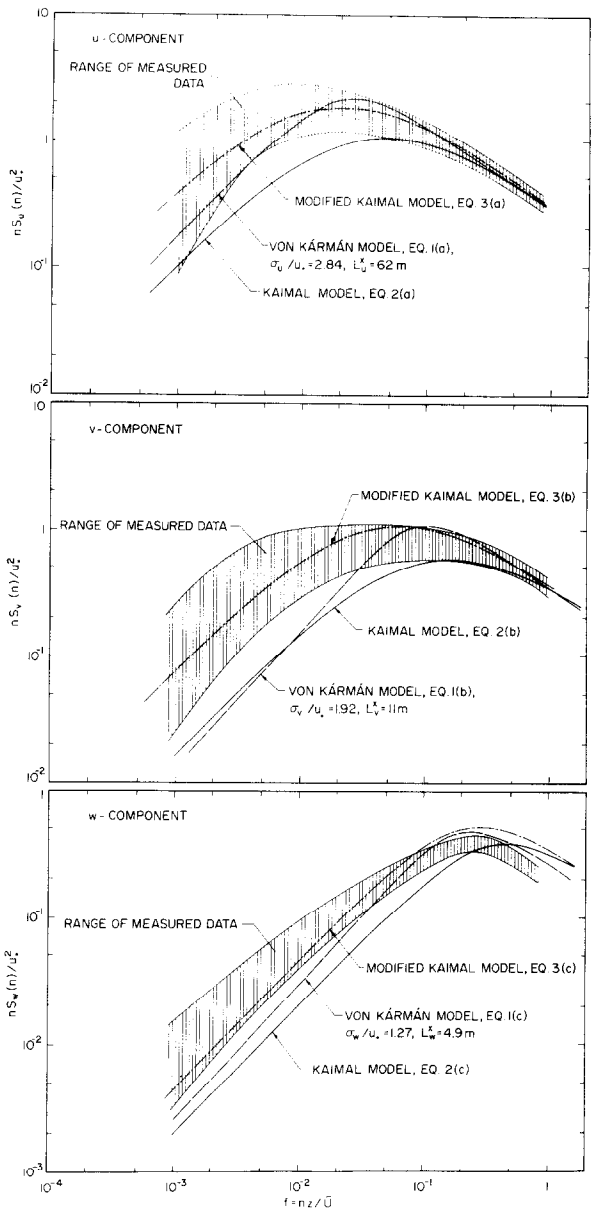

Fig. 15. Comparison of measured power spectra with model expressions. Hatched areas represent range of tower-averaged curves for data blocks 7–12.

These equations are in common use in the engineering literature and have the advantage that the integral scales L_i^x are treated as 'free' scaling parameters which are chosen to match the estimated scales for a particular height and terrain type, while maintaining constant spectral shape. The Kaimal expressions are of course more common to the meteorological literature and they do not have a free scaling

parameter. They were obtained as best-fits to surface-layer results over uniform, flat, relatively featureless terrain in Kansas and are given by

$$\frac{nS_u(n)}{u_*^2} = \frac{105f}{(1+33f)^{5/3}} \qquad 2(a)$$

$$\frac{nS_v(n)}{u_*^2} = \frac{17f}{(1+9.5f)^{5/3}} \qquad 2(b)$$

and

$$\frac{nS_w(n)}{u_*^2} = \frac{2f}{1+5.3f^{5/3}}. \qquad 2(c)$$

In Figure 15, the ranges of the observed power spectra are compared with the curves corresponding to the above model expressions. For the von Kármán curves, the block-averaged values of σ_i/u_* given in Table I were used to adjust the spectral values to the same normalization as that used for the Kaimal model and plotted in the figure. Note that for the w-component, the adjusted value of 1.27 was used for σ_w/u_* in view of the findings of Section 3.2. The measured spectral results shown in the figure for this component are uncorrected values, and their position relative to the model curves at higher frequencies is that which one would expect as a result of the known frequency-response characteristics of the vertical-component anemometers. The location of the von Kármán model curves along the frequency axis was determined by eyeball-best-fits of the model curves to the observed data. This is the so-called 'spectral fit' technique for integral scale determination which is described in Section 3.7 and which yielded the values given in Figure 15 for L_i^x.

It is clear from Figure 15 that neither von Kármán nor the Kaimal spectral model is a particularly good representation of the observed results, although the former model appears to be somewhat better than the latter at lower frequencies. The Kaimal model largely underestimates the spectral content at these frequencies for all components. On the other hand, the Kaimal model *shape* appears to be better than that of the von Kármán model, and this leads to the possibility of modifying the constants in the Kaimal model in order to obtain a better fit to the observed results. This was initially pursued by introducing two adjustable scaling parameters into each of the Kaimal model equations, one for frequency scaling (a_i) and one for magnitude scaling (b_i). Thus for the u-component, for example, we would have

$$\frac{nS_u(n)}{u_*^2} = \frac{b_u \cdot 105(a_u f)}{[1+33(a_u f)]^{5/3}}$$

and similarly for the v- and w-components, with the scaling parameters being obtained in each case from an eyeball-best-fit of the Kaimal spectral shape to the observed data. It was subsequently decided to restrict the modified expressions further by retaining in them the original model energy levels in the high-frequency inertial subrange. In this way, these expressions would approach the same limiting

values in the inertial subrange ($\sim 0.31f^{-5/3}$, $0.41f^{-5/3}$ and $0.38f^{-5/3}$ for the u-, v- and w-components, respectively) as do the original expressions, and hence the isotropic ratios of 4/3 in this region would be preserved. Such a restriction reduces the above two scaling parameters to only one and yields a modified u-component model of the form

$$\frac{nS_u(n)}{u_*^2} = \frac{105f}{[c_u + 33f]^{5/3}}$$

and similarly for the v- and w-components. Fitting such relations to the present data produced scaling parameter (c_i) values of 0.44, 0.38 and 0.44 for the u-, v- and w-components, respectively, in comparison with the Kaimal model values of 1 for all components. Thus the modified model equations are given by

$$\frac{nS_u(n)}{u_*^2} = \frac{105f}{(0.44 + 33f)^{5/3}} \qquad 3(a)$$

$$\frac{nS_v(n)}{u_*^2} = \frac{17f}{(0.38 + 9.5f)^{5/3}} \qquad 3(b)$$

and

$$\frac{nS_w(n)}{u_*^2} = \frac{2f}{0.44 + 5.3f^{5/3}}. \qquad 3(c)$$

These model curves are plotted in Figure 15 and can be seen to fit the observed data quite well over the entire frequency range, and certainly better than those of either of the other two models.

As for the reason for the higher spectral energies found in the low-frequency region of the spectra in comparison with the Kansas results, this is not entirely obvious, although the rougher terrain in the present case would seem to be a logical answer. It is noted that the modified curves in the present case bear virtually the same relationship to Kaimal's original neutral-stability curves as do his observed Kansas results for unstable flows (Kaimal *et al.*, 1972). This raises the question of possible stability effects in the present data, particularly in view of the 'excluded regions' for the u- and v-spectra discussed in Kaimal's paper and the fact that it would apparently require only a slight instability to produce the observed effect on the present data. On the other hand, the temperature data observed between 1400 and 1500 h (Section 3.1) clearly showed a slightly *positive* potential temperature gradient in the lowest 50 m, not a negative one. Since the spectra from the data blocks corresponding to this time period (i.e., blocks 1–3) fell well within the ranges shown in Figure 15 for blocks 7–12, the possibility that the observed behaviour is due to different (i.e., unstable) thermal stability for the latter data is rejected, and it would therefore appear that stability effects do not play a significant part in the observed spectral behaviour. As for possible terrain effects, the spectral results obtained by Flay (1973) over terrain very similar to that in the present case tend in general to be above the predictions of

the Kaimal model at low frequencies in a manner similar to the present results. It is therefore suggested that the observed spectral behaviour at low frequencies, relative to the Kansas results, is a logical consequence of the generally rougher gross features of the upstream terrain in the present case (i.e., trees, fences, isolated farm buildings, etc.). The use of adjustable scaling parameters in the original Kaimal spectral model allows modification of this model to take account of such effects, and it is suggested

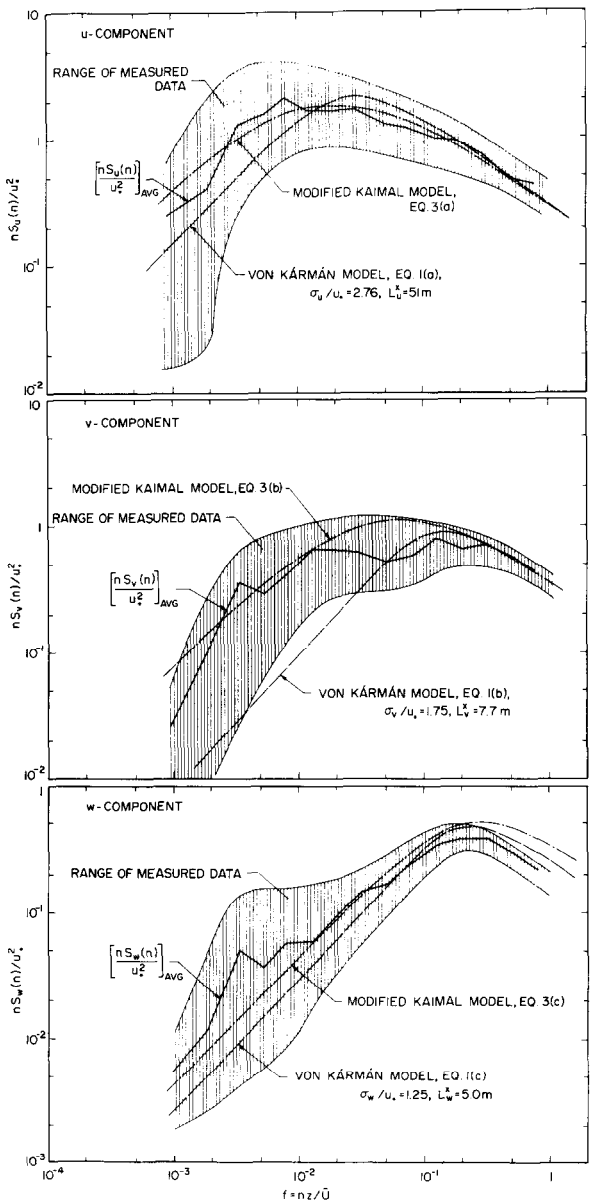

Fig. 16. Range of variation of observed power spectra over tower array for data block 12.

that it may in future be possible to represent spectra over a wide range of terrain types by using such modified expressions together with appropriate values of these 'terrain scaling' parameters. Note that in the present case, a single value of $c = 0.4$ can be used for all velocity components to produce model curves which are within about 12% of those represented by Equations (3).

The range of variation of the power spectra for all towers in data block 12 is shown in Figure 16 along with the tower-averaged spectra for the block. As in the case of the block-averaged data, the best-fit von Kármán expressions do not represent the tower-averaged curves as well as do the modified Kaimal expressions. Note that the von Kármán model for the w-component has again been adjusted upward to compensate for the low raw estimate of σ_w/u_* in Table I.

3.6. Spatial cross-correlations

For problems involving wind effects on long, horizontal structures such as suspension bridges and transmission lines, the characteristic dimensions of the turbulent eddies in the direction of the span of the structure (i.e., their 'widths') are very important, particularly for the longitudinal and vertical components. Such characteristic dimensions for eddies of all frequencies are given by the zero-time-delay cross-correlations in the lateral (y) direction for each velocity component. Results of this type were obtained in the present case from time-delayed cross-correlation curves for various combinations of towers and hence for various lateral separations. Some typical curves of this type are presented in Figure 17 for the lateral velocity component and for a number of values of separation. As expected, these curves fall toward zero with increasing magnitude of the delay-time, τ, and their maximum magnitude occurs at or very close to $\tau = 0$ (ignoring the obvious exceptions resulting

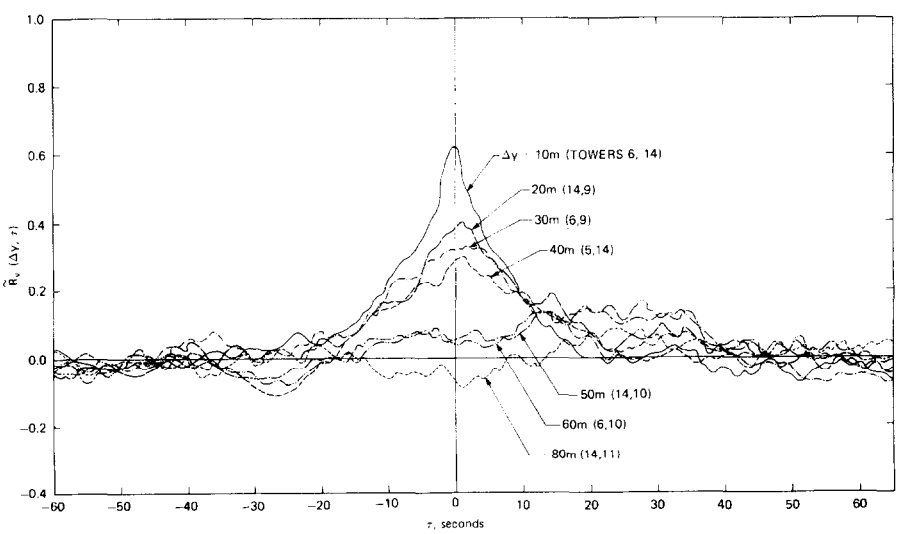

Fig. 17. Typical time-delayed cross-correlation curves for lateral velocity components and various tower combinations in data block 12.

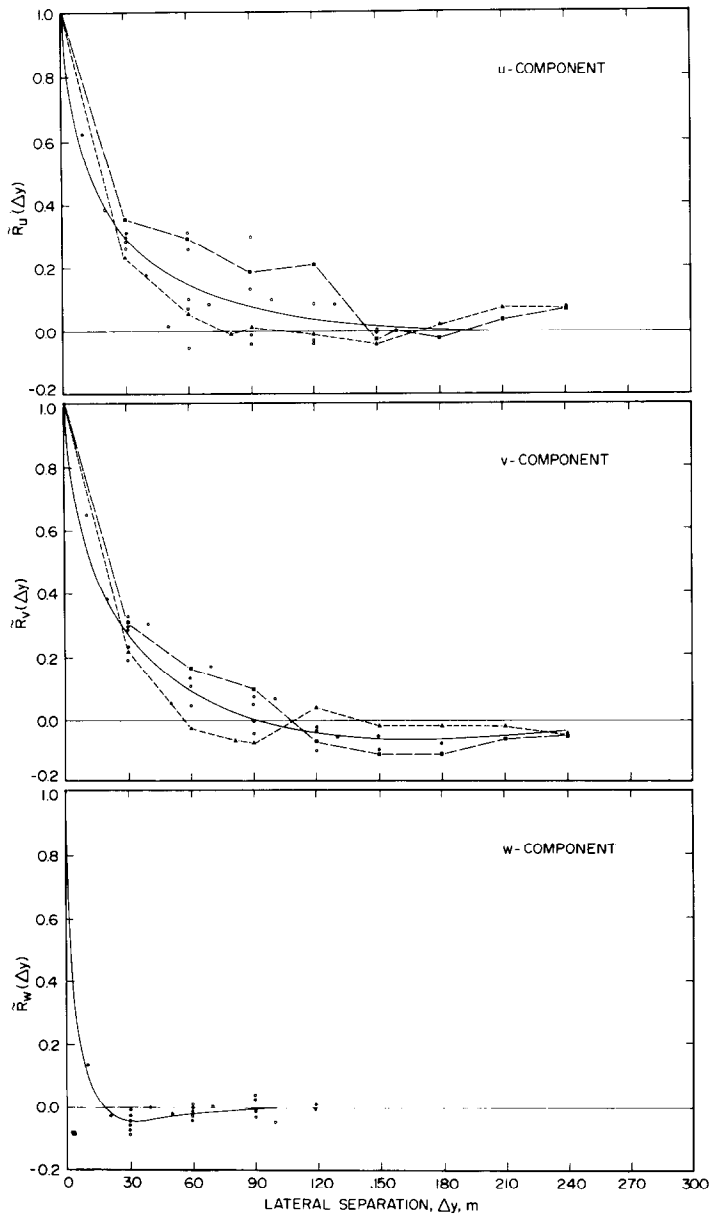

Fig. 18. Spatial cross-correlation results for lateral separations in data block 12. Solid lines are for averaged data from all tower pairs, long-dashed lines are for separations from tower 1 only and short-dashed lines are for separations from tower 11 only.

from statistical scatter). The values at $\tau = 0$ from curves of this type were used to obtain the spatial cross-correlation results presented in Figures 18 and 19.

Figure 18 displays the lateral cross-correlation results for all three velocity components and all combinations of towers in data block 12. In view of the spatial arrangement of the towers (Figure 2), there are many values of separation which

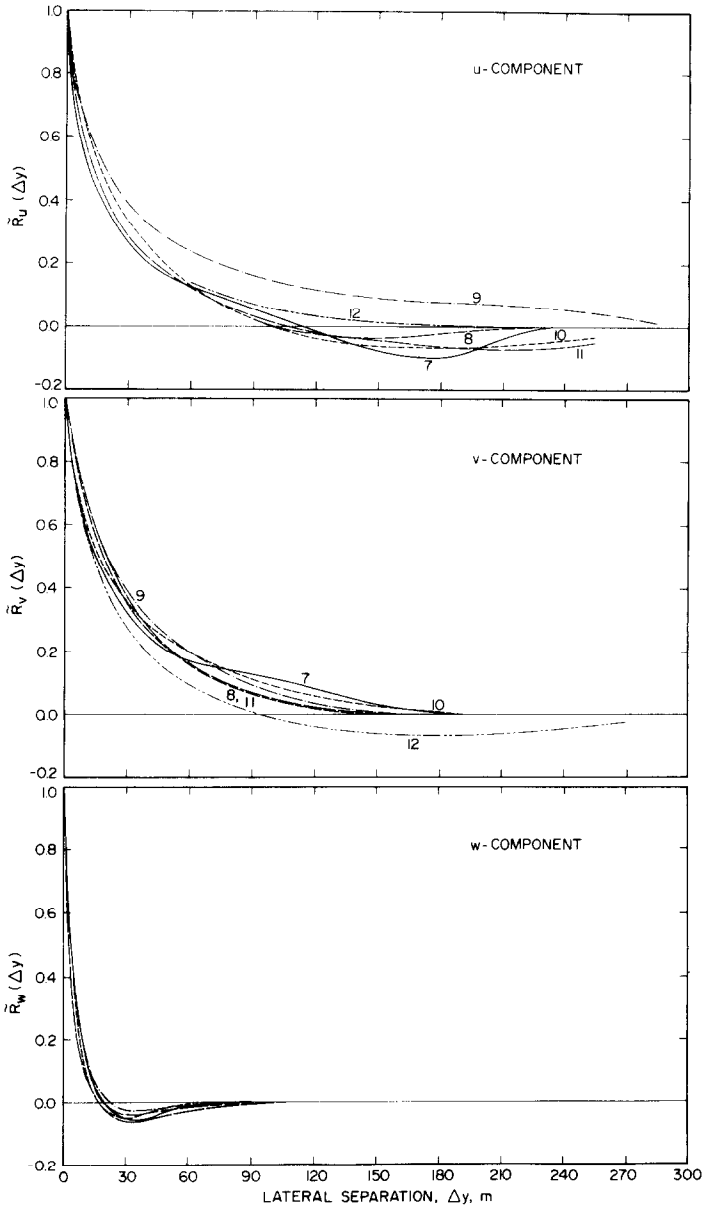

Fig. 19. Spatial cross-correlation curves from averaged data for all tower pairs in each of data blocks 7–12.

correspond to more than one pair of towers. For these separations, all the appropriate correlation values have been plotted in Figure 18. It is seen from these results that the scatter in u-component correlation values at a fixed separation is larger than that in the v- or w-component values. Similar results were observed for all other data blocks. The solid curves shown in Figure 18 have been fitted by eye to the single,

average correlation value for each separation. The two other curves for each of the horizontal components are those which join points corresponding to separations from the single tower at one or the other end of the array (i.e., tower 1 or tower 11, for these results). If the turbulence were truly homogeneous and statistical variability were negligible, these curves would coincide with the corresponding curve for the averaged data. On the other hand, any significant spatial inhomogeneity in the lateral turbulence structure which might be hidden by averaging of the data would be expected to be distinguishable in curves of this type. Such curves were therefore plotted for all data blocks, and the absence of any unusual characteristics in them was taken as further confirmation of the earlier assumption (Section 3.2) of reasonable horizontal homogeneity for these data blocks.

Cross-correlation curves from averaged data for all tower pairs in each of data blocks 7 through 12 are shown in Figure 19. The block-to-block variability in these results is seen to be fairly modest and is again smallest for the w-component. The relatively small width of the vertical gusts is obvious from the rapid drop of the w-component curves in comparison with those of the horizontal components and is demonstrated further by the corresponding integral scale values discussed in the next section.

3.7. Integral Scales

Integral scale values for atmospheric turbulence from various sources have traditionally displayed a large degree of variability. Part of this variability is a logical result of the dependence of turbulence scales on terrain characteristics, thermal stability and height above the surface. Considerable variability also results, however, from the different definitions often used for 'scales' and from different techniques used to measure them, each of which can produce widely different results for the same quantity. In the present case, the scales considered are the true integral scales of turbulence, rigorously defined as the complete integral of the appropriate correlation curve. Such scales were obtained for all velocity components by three different techniques. These are:

(i) the 'spectral fit' technique referred to in Section 3.5, in which a von Kármán spectral model is fitted to the normalized power spectrum of the velocity component, with emphasis on the usually more reliable high-frequency region of the spectrum in performing the fit. The wave number k_p^i at which the peak in the *model* spectrum occurs is then used to obtain the integral scales from the relations

$$L_u^x = 0.146/k_p^u, \qquad L_v^x = 0.106/k_p^v \quad \text{and} \quad L_w^x = 0.106/k_p^w,$$

which were shown by Teunissen (1970) to be appropriate for the von Kármán model. This technique is in effect the same as that described by Kaimal *et al.* (1972) and Kaimal (1973) for application to stable surface-layer spectra, and Taylor's hypothesis is of course implicit in converting what are actually time scales into length scales in both cases;

(ii) the 'correlation integral' technique, in which true integrations of the auto- or cross-correlation curves are carried out. This approach requires extrapolation of the curves to zero, a procedure which is of necessity rather subjective. Scales obtained using this approach are represented by the symbols l_i^x and Taylor's hypothesis is again assumed when dealing with autocorrelation curves;

(iii) an 'exponential fit' technique, in which the value of time delay or spatial separation at which the normalized correlation curve has fallen to 0.368 (i.e., e^{-1}) is taken as the integral scale value. This approach assumes an exponential shape for the correlation curves regardless of what their tails may actually look like, and hence it involves in effect a more objective extrapolation to zero than does the above approach. Scales obtained using this technique are represented by the symbols $\hat{l}_i^x$.

Figure 20 displays integral scales calculated by all three of the above techniques from the tower-averaged power spectra and autocorrelation curves for each of data blocks 7 through 12. The very large block-to-block scatter in the u- and v-component results is not untypical of atmospheric data and demonstrates part of the reason for the large variability in many published results which was referred to above. The particularly low value of l_u^x for block 11 is an inevitable result of the large negative tail in the corresponding autocorrelation curve (Figure 13). Once again, the

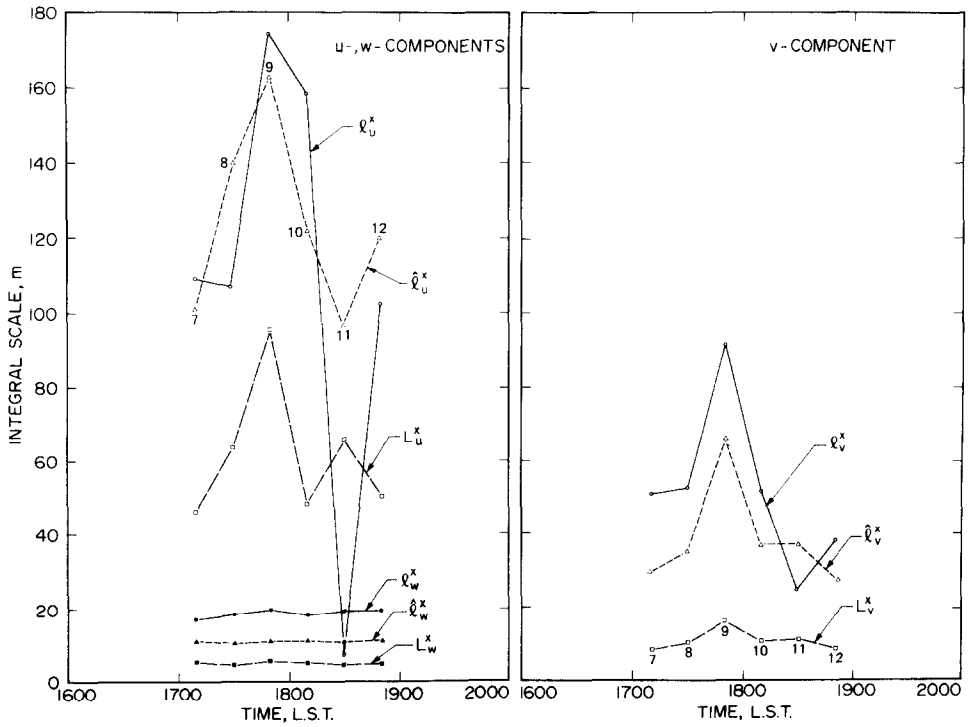

Fig. 20. Integral scales calculated by different techniques for data blocks 7–12.

vertical component results display significantly less variability than those for the horizontal components. In general, it can be seen that scales obtained using the correlation integral approach are the largest of the three techniques, those from the spectral fit approach are the smallest and those from the exponential fit approach tend to lie between them. This relationship is similar to that usually observed for atmospheric data (e.g., ESDU, 1974; Flay, 1978). Additional discussion of the

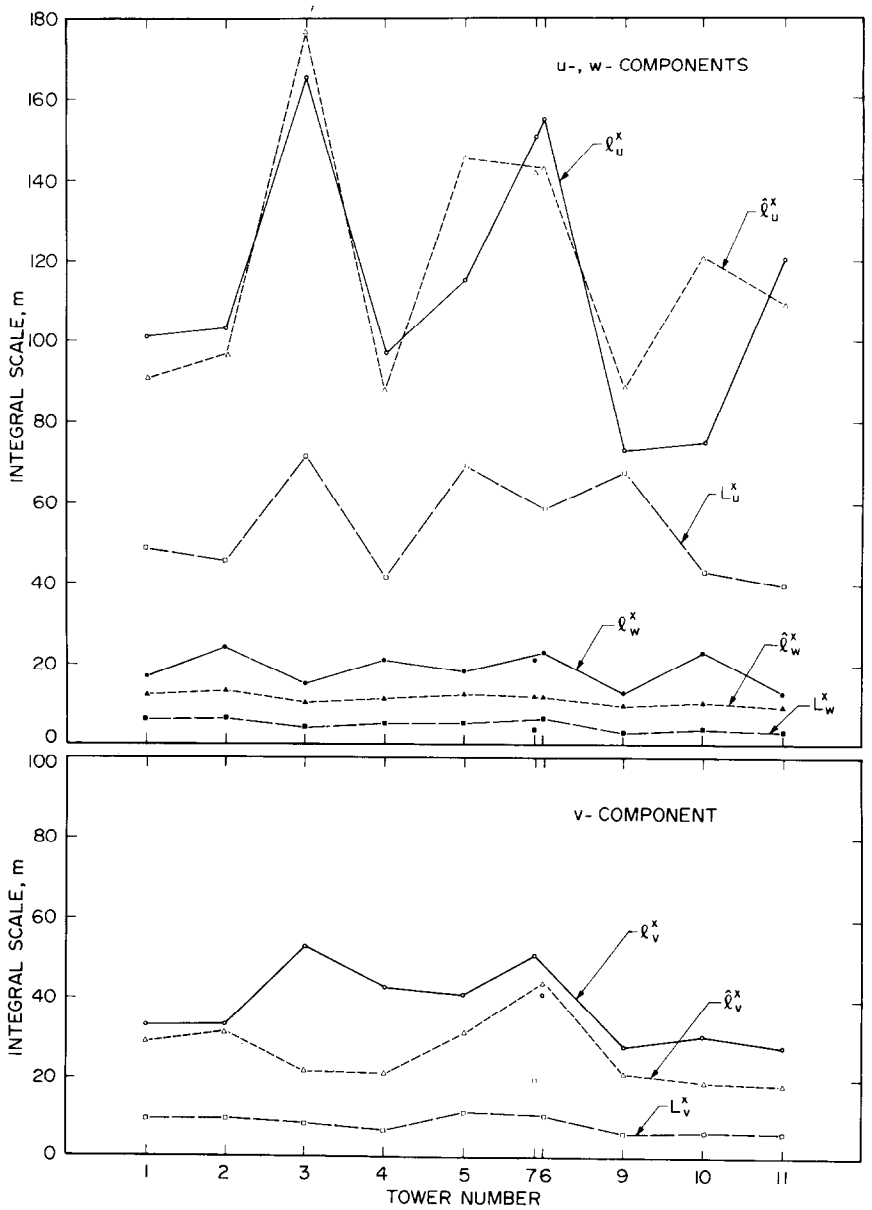

Fig. 21. Variation of integral scales over tower array for data block 12.

relative merits and difficulties of some of these approaches to scale calculation has been given by Teunissen (1970, 1972) among other authors.

The variation of integral scale values over the tower array for data block 12 is shown in Figure 21. The tower-to-tower variability is seen to be similar to the block-to-block variability displayed in Figure 20. Also, the average of the scales obtained from the power spectrum or autocorrelation curve for each tower in the array was in all cases found to be within about 5–10% of the scale value obtained from the corresponding average power spectrum or correlation curve for all the towers, i.e., 'the average of the scales was approximately equal to the scale of the averages'.

Figure 22 displays the integral scales obtained for all three components for separations in the lateral direction. These scales were calculated from the spatial cross-correlation curves of Figure 19 and are seen like them to display fairly modest block-to-block variability. As expected from the shape of the correlation curves, the correlation integral and exponential fit techniques for scale calculation give similar results.

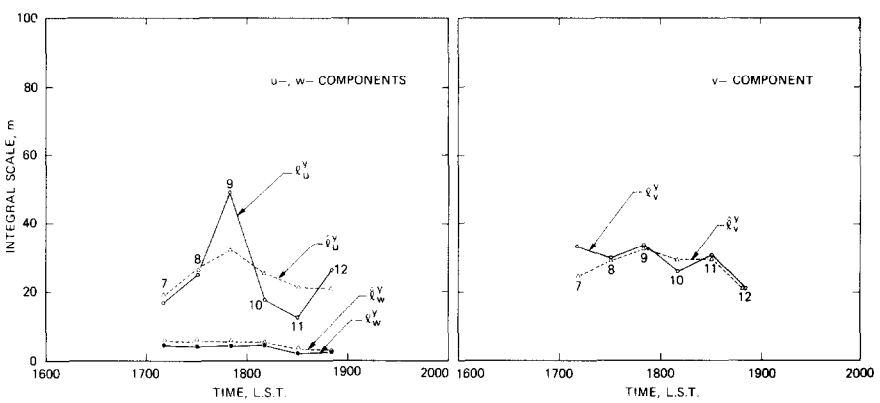

Fig. 22. Integral scales for lateral separations for data blocks 7–12.

Block-averaged values for all the scales presented in Figures 20 and 22 are tabulated in Table II along with corresponding values suggested by the atmospheric models referred to earlier and some other comparable results from the literature. The large number of blanks in this table for all but the present results and those of Flay (1978) is perhaps a fair indication of the relative sparseness of full-scale results for many of these scales. Insofar as model predictions are concerned, it is clear from the table that most of the values suggested by ESDU (1975) are in considerably better agreement with the observed results than those suggested by Counihan (1975), as was found also to be the case for the Reynolds stress and variance results discussed in Section 3.3. The results of Flay (1978) over similar terrain (but not snow-covered) are also in relatively good agreement with the present data and with the predictions of the ESDU model. (Note that the extremely low value of l_u^x for data

block 11 (see Figure 20) has been excluded from the averaging process in obtaining the tabulated block-average value in Table II). The results of Shiotani and Iwatani (1976) and Shiotani *et al.* (1978) were obtained during typhoon conditions at a height of 40 m above a coastal site in Japan for both on-shore and off-shore winds. Thus, as expected, their values are all somewhat larger than the present results. Harris's (1972) data were obtained at a site similar to the present one and also agree well with the present observations.

TABLE II

Comparison of average integral scale values (m) with idealized models and other results

	Present results, average of blocks 7–12	ESDU (1975), $z_0 \approx 0.8$ cm	Counihan (1975), $z_0 \approx 1$ cm	Flay (1978), $z_0 \approx 3$ cm	Shiotani and Iwatani (1976), Shiotani *et al.* (1978), $z = 40$ m		Harris (1972), $z_0 \approx 0.3$ cm
					Land fetch	Sea fetch	
L_u^x	62	78	~200	83	–	–	–
L_v^x	11	25	–	15	–	–	–
L_w^x	4.9	3.8	4.4	6.5	12	12	–
l_u^x	130*	–	–	144	135±29	195±55	130
l_v^x	52	–	–	66	–	–	66
l_w^x	18	–	–	19	–	33±12	–
l_u^y	24	35	~70	24	–	–	35
l_v^y	29	–	–	27	–	–	–
l_w^y	3.5	3.8	–	5.0	–	–	–
$\hat{l}_u^x$	124	–	–	97	154±60	204±61	–
$\hat{l}_v^x$	39	–	–	51	–	–	–
$\hat{l}_w^x$	11	–	–	19	–	–	–
$\hat{l}_u^y$	24	–	–	25	60±20	50±25	–
$\hat{l}_v^y$	28	–	–	26	–	–	–
$\hat{l}_w^y$	4.9	–	–	5.1	–	13±3	–

* excluding data block 11.

The integral scale values of Table II can of course be used to obtain an estimate of the relative physical dimensions of the turbulent eddies in the longitudinal and lateral directions. For consistency and in view of the true definition of integral scale, we use only the correlation-integral scale values for this purpose and obtain

$$l_u^x/l_u^y \approx 5.4\,, \qquad l_v^x/l_v^y \approx 1.8 \quad \text{and} \quad l_w^x/l_w^y \approx 5.1.$$

Thus we see as expected that the turbulent eddies are elongated in the along-wind direction and that this elongation is considerably more significant for the u-component than for the v-component. Similar findings were obtained by Panofsky (1962) at a height of 2 m in stable and neutral flows, although his observed degree of elongation tended to be somewhat larger than in the present case for both

components (i.e., ratios of about 8 and 3 as opposed to the above values of 5.4 and 1.8 for the u- and v-components, respectively). Panofsky's w-component results also implied elongation of the eddies in the longitudinal direction, although the data did not permit the determination of a quantitative estimate of this elongation. The present results yield a factor of about 5.1 and hence indicate an elongation which is about the same in magnitude as that indicated by the u-component. In isotropic turbulence, of course, the above three ratios would be 2, 0.5 and 1, respectively.

The ratios of the integral scales for the three velocity components for separations in the longitudinal direction only are given by

$$l_u^x/l_v^x \approx 2.5\,, \qquad l_u^x/l_w^x \approx 7.2 \quad \text{and} \quad l_v^x/l_w^x \approx 2.9.$$

The corresponding ratios for isotropic turbulence are 2, 2 and 1, respectively, thereby emphasizing the extremely small scale of the w-component fluctuations. For separations in the lateral direction only, the ratios

$$l_u^y/l_v^y \approx 0.8\,, \qquad l_u^y/l_w^y \approx 6.9 \quad \text{and} \quad l_v^y/l_w^y \approx 8.3$$

compare with isotropic values of 0.5, 1 and 2, respectively. Finally, the ratio $l_u^x/l_v^y \approx 4.5$, in comparison with the isotropic value of 1, is yet another indication of the elongation of eddies in the longitudinal direction. Scale ratios of the type discussed here can of course be obtained for any of the other atmospheric observations of Table II simply by using the scale values presented therein. In general, most of these ratios are similar to those presented above.

Finally, from Table II, it can be determined that, on average, the relative magnitudes of the integral scales obtained by the three techniques discussed in this paper are given by

$$l_u^x \approx \hat{l}_u^x \approx 2.1\, L_u^x\,,$$

$$l_v^x \approx 1.3\, \hat{l}_v^x \approx 4.6\, L_v^x\,,$$

$$l_w^x \approx 1.6\, \hat{l}_w^x \approx 3.7\, L_w^x\,,$$

and

$$l_u^y \approx \hat{l}_u^y\,, \qquad l_v^y \approx \hat{l}_v^y \quad \text{and} \quad l_w^y \approx 0.7\, \hat{l}_w^y\,.$$

4. Conclusions

Detailed analysis has been carried out on a 5-h data set obtained from a horizontal array of fifteen 11-m towers at a time when the wind was blowing perpendicular to the tower array at about 10 m s^{-1}. The ground was snow-covered and the boundary layer was virtually neutrally stable for this data set. The main conclusions of the analysis are summarized as follows:

(1) Considerable tower-to-tower variability was observed in most of the measured wind and turbulence characteristics. While most of this variability was statistical in

nature, some of the observed spatial patterns could clearly be attributed to the detailed features of the upstream terrain for each of the two slightly different mean wind directions encountered during the measurement period.

(2) Block-to-block variability of the tower-averaged results for each data block was in most cases similar in magnitude to the tower-to-tower variability within the data blocks.

(3) Surface shear stress, roughness length and turbulence intensities were in good agreement with expected values for terrain of this type. Predictions of the engineering model of ESDU (1974) tended to show better agreement with the present results than did those of Counihan (1975).

(4) Observed power spectra for all three velocity components displayed significantly more energy at lower frequencies than predicted by the model of Kaimal *et al.* (1972) for the flow over flat, featureless terrain. It is felt that this difference is a logical result of the generally rougher gross features of the upstream terrain in the present case. The von Kármán spectral model recommended by Teunissen (1970) and ESDU (1974, 1975) fitted the observed results better than did the Kaimal model in terms of magnitude, but not in terms of spectral shape. A modified version of the Kaimal model was produced by adding a scaling parameter to each of the spectral equations and evaluating these parameters from the observed data. These modified expressions fitted the observed results better than either of the other two models, and it has been suggested that it may be possible to represent the power spectra over a wide range of terrain types by using these expressions with appropriate values of such 'terrain scaling' parameters.

(5) Integral scales of turbulence obtained by three different techniques displayed a great deal of block-to-block and tower-to-tower variability. In general, the spectral-fit approach yielded the smallest value for a particular scale, the correlation-integral approach produced the largest value and the exponential-fit value usually fell between the two.

(6) Block-averaged values for integral scale were in reasonable agreement with similar available atmospheric observations and with most of the predictions of the ESDU (1975) model. The model of Counihan (1975) considerably overestimated the observed values of scale for the longitudinal component.

(7) Turbulent eddies in neutrally-stable flow over rural terrain are elongated in the longitudinal direction, and this elongation is larger for the u-component than for the v-component. These findings are similar to those of Panofsky (1962) although the magnitude of the elongation in the present case was somewhat smaller than he observed. The elongation indicated by the w-component was similar in magnitude to that observed for the u-component.

Acknowledgments

The author wishes to acknowledge the large contributions of Mr L. M. Watt in producing the data analysis programs in use at this facility and of Mr K. O. Vanek in the reduction of much of the raw data. The useful suggestions made by Dr P. A. Taylor during a critical review of the manuscript are also gratefully acknowledged.

References

Busch, N. E., Tennekes, H., and Panofsky, H. A.: 1973, 'Turbulence Structure in the Planetary Boundary Layer', *Boundary-Layer Meteorol.* **4**, 213–264.

Clarke, R. H.: 1970, 'Observational Studies in the Atmospheric Boundary Layer', *Quart. J. Roy. Meteorol. Soc.* **96**, 91–114.

Counihan, J.: 1975, 'Adiabatic Atmospheric Boundary Layers: A Review and Analysis of Data from the Period 1880–1972', *Atmos. Envir.* **9**, 871–905.

Dyer, A. J., Hicks, B. B., and Sitaraman, V.: 'Minimizing the Levelling Error in Reynolds Stress Measurement by Filtering', *J. Appl. Meteorol.* **9**, 532–534.

Elderkin, C. E., Powell, D. C., Dunbar, A. G., and Horst, T. W.: 1972, 'Take-off and Landing Critical Atmospheric Turbulence (TOLCAT)—Experiments and Analysis', Tech. Rept. AFFDL-TR-71-172, Wright–Patterson Air Force Base, Ohio, 283 pp.

Engineering Sciences Data Unit: 1974, 'Characteristics of Atmospheric Turbulence Near the Ground, Part II', ESDU Item 74031, Regent St., London, 29 pp.

Engineering Sciences Data Unit: 1975, 'Characteristics of Atmospheric Turbulence Near the Ground, Part III', ESDU Item 75001, Regent St., London, 27 pp.

Flay, R. G. J.: 1978, 'Structure of a Rural Atmospheric Boundary Layer Near the Ground', Ph.D. Thesis, University of Canterbury, Christchurch, N.Z., 400 pp.

Harris, R. I.: 1972, 'Measurement of Wind Structure', Paper presented at the Symposium on External Flows, University of Bristol, July 4–6, 31 pp.

Hicks, B. B.: 1972, 'Propeller Anemometers as Sensors of Atmospheric Turbulence', *Boundary-Layer Meteorol.* **3**, 214–228.

Horst, T. W.: 1973, 'Corrections for Response Errors in a Three-Component Propeller Anemometer', *J. Appl. Meteorol.* **12**, 716–725.

Kaimal, J. C. and Haugen, D. A.: 1969, 'Some Errors in the Measurement of Reynolds Stresses', *J. Appl. Meteorol.* **8**, 825–827.

Kaimal, J. C., Wyngaard, J. C., Izumi, Y., and Coté, O. R.: 1972, 'Spectral Characteristics of Surface Layer Turbulence', *Quart. J. Roy. Meteorol. Soc.* **98**, 563–589.

Kaimal, J. C.: 1973, 'Turbulence Spectra, Length Scales and Structure Parameters in the Stable Surface Layer', *Boundary-Layer Meteorol.* **4**, 289–309.

Kaimal, J. C., Wyngaard, J. C., Haugen, D. A., Coté, O. R., and Izumi, Y.: 1976, 'Turbulence Structure in the Convective Boundary Layer', *J. Atmos. Sci.* **33**, 2152–2169.

Lumley, J. L. and Panofsky, H. A.: 1964, *The Structure of Atmospheric Turbulence*, Interscience, Wiley, N.Y.

Panofsky, H. A.: 1962, 'Scale Analysis of Atmospheric Turbulence at 2 m', *Quart. J. Roy. Meteorol. Soc.* **88**, 57–69.

Panofsky, H. A.: 1977, 'Wind Structure in Strong Winds Below 150 m', *Wind Engineering* **1**, 91–103.

Perry, S. G., Norman, J. M., Panofsky, H. A., and Martsolf, J. D.: 1978, 'Horizontal Coherence Decay Near Large Mesoscale Variations in Topography', *J. Atmos. Sci.* **35**, 1884–1889.

Ropelewski, C. F., Tennekes, H., and Panofsky, H. A.: 1973, 'Horizontal Coherence of Wind Fluctuations', *Boundary-Layer Meteorol.* **5**, 353–363.

Shiotani, M. and Iwatani, Y.: 1976, 'Horizontal Space Correlations of Velocity Fluctuations During Strong Winds', *J. Meteorol. Soc. Japan* **54**, 59–67.

Shiotani, M., Iwatani, Y., and Kuroha, K.: 1978, 'Magnitudes and Horizontal Correlations of Vertical Velocities in High Winds', *J. Meteorol. Soc. Japan* **56**, 35–42.

Teunissen, H. W.: 1970, 'Characteristics of the Mean Wind and Turbulence in the Planetary Boundary Layer', UTIAS Review 32, University of Toronto, Canada, 57 pp.
Teunissen, H. W.: 1972, 'Simulation of the Planetary Boundary Layer in a Multiple-Jet Wind Tunnel', UTIAS Report 182, University of Toronto, Canada, 171 pp.
Teunissen, H. W.: 1977, 'A Measurement and Analysis Facility for Full-Scale Atmospheric Wind and Turbulence Data', Internal Report MSRB-77-2, Atmospheric Environment Service, Toronto, 78 pp.
Teunissen, H. W.: 1979, 'Measurements of Planetary Boundary Layer Wind and Turbulence Characteristics over a Small Suburban Airport', *J. Ind. Aerodynam.* **4**, 1–34.